The Selective Laser Sintering of Polycarbonate

M. Berzins, T.H.C. Childs (2), G.R. Ryder, University of Leeds, U.K.
Received on January 8, 1996

Abstract

This paper investigates thermal modelling of the selective laser sintering process for amorphous polycarbonate powders. The aim is to develop a simulation for process accuracy and control which are key areas of developement for the new layer manufacturing rapid prototyping technologies. A state-of-the-art adaptive mesh 2D finite difference code is used simultaneously to consider heating and sintering and its results compared with a classical moving heat source model and with experiments. The analysis shows that the change of material thermal properties with temperature and particularly with position as densification takes place must be included for accurate prediction of both densification and of the phenomenon known as 'bonus z'. The work forms a basis for moving to a 3D simulation.

Keywords : Rapid prototyping, Sintering, Thermal modelling

1. Introduction

Rapid prototyping by layer manufacturing or solid free form fabrication, first reviewed by Kruth (1991), has continued to find new applications in the last few years, from concept to functional prototypes and now for prototype tooling. However, even the more accurate commercial processes, Stereolithography and Selective Laser Sintering (SLS), are not as accurate as machining or moulding (Childs and Juster, 1994). This paper reports theoretical modelling and experimental studies of SLS. The aim is to create a process simulation that will aid SLS manufacturing accuracy and control.

In the SLS process, a rastering infra-red laser beam heats the surface of a powder bed, to fuse the powder in a cross-section that matches that of a prototype being replicated. The surface is then covered with another layer of powder and the cycle is repeated. The current fused layer is bonded to that beneath to build up the 3D shape of a part. The powder is commonly a polymer, for example amorphous polycarbonate that is used for sacrificial patterns in investment casting, or crystalline nylon for functional plastic parts.

In a commercially available machine, the whole bed is heated to almost the polymer's melting or glass transition temperature (154°C for polycarbonate). The laser (with power, scan speed and scan spacing that can be varied and a beam diameter of 0.4 mm) supplies only the energy needed to increase the temperature into the sintering range. A common layer thickness is 0.125 mm. In the horizontal (x,y) plane of the powder bed surface, beam offsets are applied to obtain coincidence between the actual and designed section shape, but random errors can create a range of ± 0.2 mm inaccuracies. In the z direction, a systematic error, known as 'bonus z', can occur on downward facing horizontal surfaces: in standard conditions powder can be sintered too deep, to create an oversize in z of typically 0.5 mm. On top of these sintering errors, shrinkage and distortion can occur on cooling the powder bed back to room temperature.

In this paper, the SLS of polycarbonate is considered. As it is amorphous, there is no latent heat to be accounted for in thermal modelling. It is demonstrated that it is essential to take into account the variation of the polycarbonate's thermal properties with temperature and densification in order accurately to predict its sintering. The physical basis now exists for creating a 3D thermal model of the SLS of polycarbonate parts.

2. Theory

Figure 1, in which x and y are in the plane of the powder bed surface, shows the simple geometry that is currently the subject of modelling. A rectangular block ABCD of width AB = w is created by a rastering laser beam, of power P and spot diameter d. The beam travels with speed U in the x-direction, increments its track by a scan spacing s, and travels back in the -x direction, also at speed U. This cycle is repeated from the starting edge AB to the end CD of the block. The modelling has two elements: calculating the temperature / time history of elements beneath the surface; and determining the consequent densification caused by sintering.

When, as is always the case, s < d, and if the cycle time 2w/U is less than the time d^2/κ for heat to

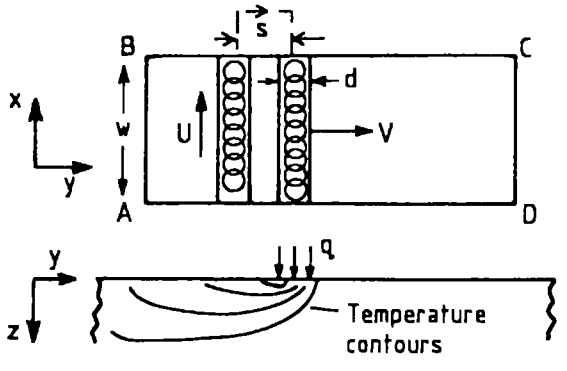

Figure 1. Plan and side view of sintering a block ABCD.

diffuse d (where κ is the thermal diffusivity), the laser spot may be replaced by a rectangular blade source of side d x w, of power q per unit area, sweeping across the block with speed V in the y direction, where, for the blade and the actual laser source to transmit the same energy density to the powder, in the same time (Childs et al., 1994)

$$V = sU/w; \qquad q/V = (P\,Us)\,d. \tag{1}$$

The temperature/time (T / t) history in the powder bed caused by the moving blade heat source is calculated by solving the heat conduction equation

$$\rho C\frac{\partial T}{\partial t} = k\nabla^2 T + \frac{\partial k}{\partial T}\left\{\left(\frac{\partial T}{\partial x}\right)^2 + \left(\frac{\partial T}{\partial y}\right)^2 + \left(\frac{\partial T}{\partial z}\right)^2\right\} + \frac{\partial k}{\partial x}\frac{\partial T}{\partial x} + \frac{\partial k}{\partial y}\frac{\partial T}{\partial y} + \frac{\partial k}{\partial z}\frac{\partial T}{\partial z} \tag{2}$$

(k is conductivity, ρ is density and C is specific heat). Terms for k varying with temperature and position (due to densification) are a key feature of the calculation. k (W/m°K) and C (J/kg) for the solid have been taken to vary with temperature / °K (Nelson et al.,1993) as

$$C = 935 + 2.28T;\ k_{solid} = 0.0251 + 0.0005T. \tag{3}$$

k for the powder has been assumed to vary in proportion to its density, so that

$$k = k_{solid}(\rho/\rho_{solid}) \tag{4}$$

Then, in equation 2, from equations 3 and 4

$$\frac{\partial k}{\partial T} = 0.0005\frac{\rho}{\rho_{solid}};\qquad \frac{\partial k}{\partial x(y\text{ or }z)} = \frac{k_{solid}}{\rho_{solid}}\frac{\partial \rho}{\partial x(y\text{ or }z)} \tag{5}$$

Sintering densification has been assumed to follow (Nelson et al, 1993)

$$\frac{d\rho}{dt} = (\rho_{solid} - \rho)\,A\exp(-E/RT) \tag{6}$$

where $A = 8.84\times10^{16}\ s^{-1}$ and E/R = 21,000.

3. Solution Circumstances and Strategies.

Equations 2 to 6 have been solved simultaneously for two circumstances. The creation of a single sintered layer block has been modelled to study the 'bonus z' phenomenon. The sintering of multi-layer blocks has been modelled to determine the effect of build parameters (P, U and s) on densification. Figure 2 shows detail of the building of a 4-layer block that can be used to explain both the single and multi-layer models. At the start, a first layer of powder densifies to a depth Δh_1 below its initial surface. If the density variation with depth is $\rho(z)$ without considering the effect of shrinking, and the initial powder density is $\rho_{initial}$, the layer shrinks to dh_1 given by

$$dh_1 = \int_0^{\Delta h_1}\frac{\rho_{initial}}{\rho(z)}\,dz \tag{7}$$

When a new layer of powder 0.125 mm thick is spread over the initial surface, it has a greater thickness Δh_2 over the first layer. The new layer shrinks to dh_2 on sintering. The spreading, sintering and shrinking cycle continues layer by layer: for the ith layer

$$dh_i = \int_0^{\Delta h_i}\frac{\rho_{initial}}{\rho(z)}\,dz \tag{8}$$

A steady state is reached when dh_i = 0.125 mm. Then, by mass conservation, the average density of a layer is

$$\rho_{average} = (\Delta h_i/dh_i)\,\rho_{initial} \tag{9}$$

Density profiles $\rho(z)$ have been calculated for both the single and multi-layer cases using both analytical and numerical temperature calculation stategies.

Analytically, a classical result for a rectangular moving heat source (Jaeger, 1942) has been used, valid for constant thermal properties. In this case temperature rise is

$$T = \frac{q}{V}\frac{\kappa k}{2\sqrt{2\pi}}\int_0^{V^2t/2\kappa}\frac{e^{-Z^2/2u}}{\sqrt{u}}\left(\operatorname{erf}\frac{X+B}{\sqrt{2u}} - \operatorname{erf}\frac{X-B}{\sqrt{2u}}\right)x\left(\operatorname{erf}\frac{Y-L+u}{\sqrt{2u}} - \operatorname{erf}\frac{Y-L+u}{\sqrt{2u}}\right)du \tag{10}$$

where

$$X = \frac{Vx}{2\kappa},\quad Y = \frac{Vy}{2\kappa},\quad Z = \frac{Vz}{2\kappa},\quad L = \frac{Vd}{4\kappa}\ \text{ and }\ B = \frac{Vw}{4\kappa}.$$

Variable thermal properties have been accomodated by choosing appropriate average values. For a single layer calculation, k for unsintered powder has been assumed and ρ has also been taken to be that of the unsintered powder because these give the greatest sintering depth. Temperature / time histories from equation 10 have been substituted in equation 6 to obtain, after integration, sintered $\rho(z)$ contours. Finally, equation 7 has been used for the shrinkage associated with the densification.

Equation 10 with 6 has also been used to predict densification of multi-layer blocks. In this case two approaches have been taken for appropriate thermal properties. Firstly equation 3 has been used to estimate values for C_p and k_{solid} for T = 300 to 800°K and equation 4 to determine values of k for values of ρ from that for unsintered powder to that for solid material. The sensitivity of temperature / densification and $\rho_{average}$, from equation 9, to these choices has been studied.

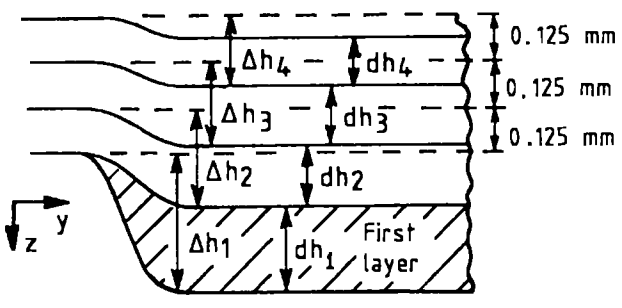

Figure 2. Schematic view of building a multi-layer part.

A self-consisitent iterative method has also been used for thermal properties. An input mean density has been used to determine k from equation 4; and the thermal and densification calculations have been employed to obtain $\rho_{average}$ from equation 9. The input density has been altered until it has equalled the ouput $\rho_{average}$.

The second strategy is to use a state-of -the-art adaptive mesh finite difference code, VLUGR2 for 2D or VLUGR3 for 3D problems (Blom and Verwer, 1993), to solve equations 2 to 6. The problem interface in VLUGR allows k to vary with both temperature and position. Error control in both space and time is used to calculate numerical solutions to a required accuracy. For the numerical experiments to be described here, the 2D code was used, with a spatial tolerance of 0.00001, resulting in spatial meshes with a maximum of 6 nested levels and typically with 23,000 mesh points.

The code was used to solve from a starting time t = 0 to the establishment of a steady state. For sintering a single layer, the density at t = 0 is the initial powder density and ρ(z) contours are the output; calculating the shrunk thickness from equation 7 is a post-processing operation. For a multi-layer part, the density at t = 0 is the initial powder density for the layer currently being sintered and is the distribution calculated in previous passes for lower layers. The variation of dh from layer 1 to the steady state and $\rho_{average}$ from equation 9 is calculated.

4. Experimentation

Blocks ABCD (figure 1) have been made with width w = 25 mm, length 100 mm and 1, 2, 3, 5, 10, 20 and 50 layers thick, with P = 11W, U = 860 mm/s and s = 0.203 mm. The powder bed ambient temperature was 154°C, the beam diameter d was 0.4 mm and the layer thickness was 0.125 mm.The thicknesses of these blocks were measured by a micrometer to determine dh values (figure 2).

Equation 10 suggests temperature rises should depend on q/V. Equation 1 indicates q/V depends on P/(Us). Further blocks were sintered with width w = 25 mm, length 100 mm and 50 layers thick. P was varied from 6 to 14W, U from 517 to 1206 mm/s and s from 0.102 to 0.406 mm, giving values of P/(Us) from 0.034 to 0.125 J/mm^2. The densities of these blocks were found by dividing their measured weights by their measured volumes.

Modelling requires a value for the unsintered powder bed density. 15 vertical hollow cylinders, 22 mm internal diameter and 15 mm height, each with a closed bottom, were sintered at different places in the build volume. Afterwards each was carefully removed from the powder bed, carrying inside it a sample of undisturbed powder. Powder density was estimated by removing the powder from the cylinder, weighing it, and estimating its volume in the powder bed from the internal volume of the cylinder.

5. Modelling and Experimental Results

The fifteen measurements give powder bed density to be 485 ± 20 kg/m^3.

Predicted sub-surface density variations for sintering a single layer block in the conditions described in section 3 are shown in figure 3. Part a is from using equation 10 with unsintered powder thermal properties (k_{solid} and C were given values for 600°K), part b is the finite difference calculation result. Estimates of layer thickness after accounting for shrinkage (equation 7) are marked 'shrunk depth'. The finite difference calculations predict a much thicker layer: this is due to thermal properties both varying with temperature and position (density) but the position effect is the greater.

Experimental measurements of layer thickness from multi-layer blocks are shown in figure 4. These show that the steady state value of 0.125 mm is established by the third layer. Theoretical predictions are included as the solid lines: the finite difference calculation agrees with experiment, while the analytical result is totally inadequate. It has been observed that for the multi-layer finite difference calculation it is the increased heat capacity rather than the increased conductivity of the previously sintered layers that more influences the prediction of dh.

Single layer finite difference calculations have been carried out for other sintering conditions. Density

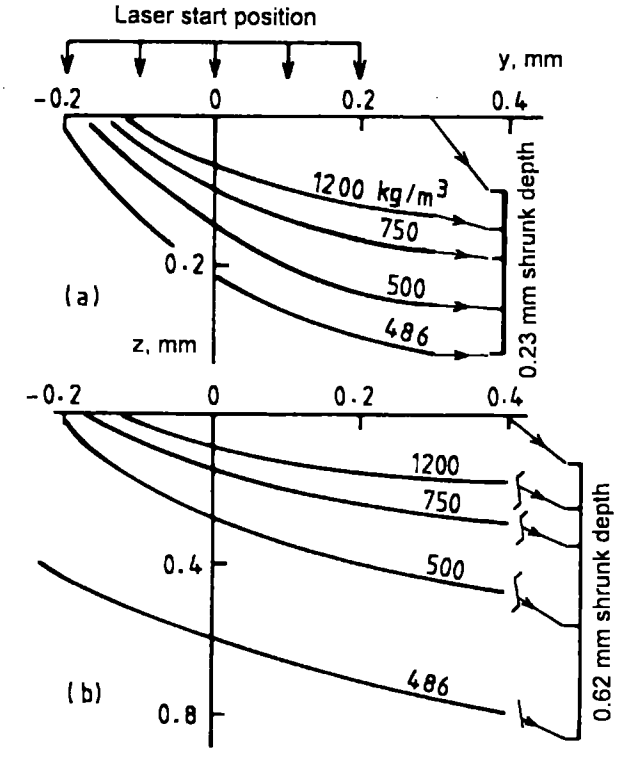

Figure 3. (a) analytical and (b) finite difference single layer ρ(z) variations, conditions described in text.

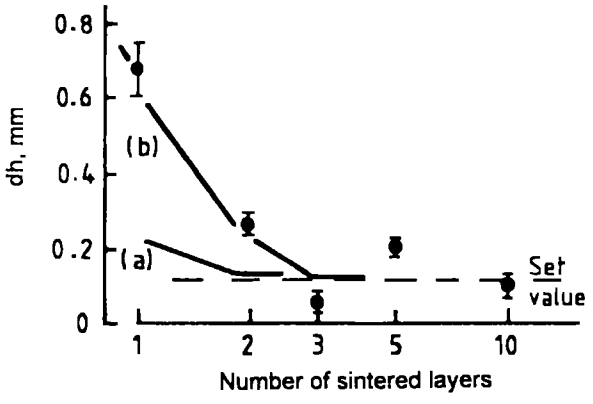

Figure 4. dh variation with layer number :expt. (•) and theory (— a, analytical and b, finite difference).

contours are shown in figure 5. The strong influence of P/(Us) on 'bonus z' is clear. It is also seen how densification extends further outside the laser start position the larger is P/(Us), showing how beam offset should be increased with increasing P/(Us).

Figure 6 compares experiments and theories for the dependence of density on P/(Us), for 50-layer blocks. In part a, a range of different predictions results from different thermal property assumptions in the analytical temperature calculation. The dashed lines marked 'P' and 'S' come from assumed room temperature powder and solid thermal properties respectively. The 'P' line predicts greater sintering than is observed and is why, in the single layer sintering calculation of figure 3a, powder

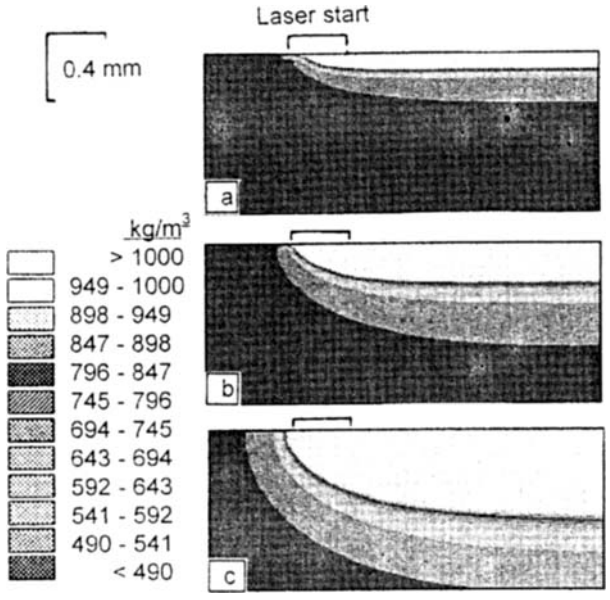

Figure 5. Predicted single layer densification for P/(Us) of (a) 0.034, (b) 0.062 and (c) 0.113 J/mm^2.

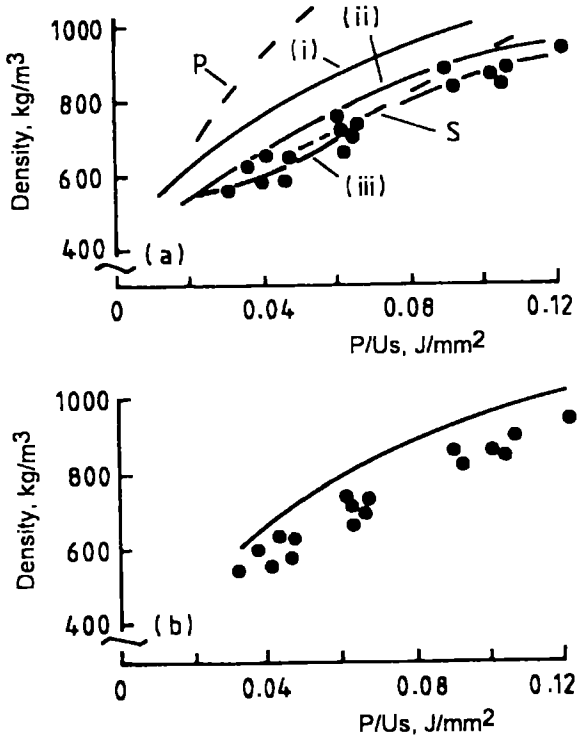

Figure 6. Density dependence on P/(Us): expt. (•) and theory (a, analytical and b, finite difference).

properties were assumed, to give an extreme prediction. The solid lines(i) to (iii) are all the result of the analytical self-consistent iterative calculation described in section 2. For line (i) T = 300°K was used in equation 3. For lines (ii) and (iii) which span the experimental results, T was taken as 600 and 800°K.

Figure 6b shows that the multi-layer finite difference calculation (the solid line) consistently over estimates experiment, but only by a small amount.

6. Discussion and Conclusion

Two thermal calculation methods have been compared for their suitability for simulating SLS. Classical moving heat source theory with a sintering model can predict average densities of multi-layer blocks if a self-consistent choice of mean thermal properties is made, but cannot correctly predict single layer sintering. The finite difference calculation can predict single layer behaviour but slightly overestimates mult-layer density.

The two methods compared show that the variation of thermal properties with position, due to densification, is critical to the transport of heat in sintering. For sintering the first layer of a block, thermal conductivity variation with position is important. For subsequent layers, the increased heat capacity of previously sintered layers is also important. The variation of thermal properties with temperature has a measurable but less significant effect. Nelson et al. (1993) came to a similar conclusion from 1D modelling. Why the finite difference method slightly overestimates multi-layer densification is not currently understood

In this paper, the simultaneous solution of heat conduction and sintering equations, fully allowing for variation of thermal properties with temperature and sintering, has been achieved by a finite difference calculation. At this time, only 2D cases have been solved, but code exists for a 3D extension. It is planned to attempt 3D solutions, once the mult-layer density discrepancy is resolved, as the next stage of the programme's aim: creating a simulation tool to aid SLS manufacturing accuracy and control.

Acknowledgement

The University of Leeds Keyworth Institute is providing a research studentship for one of us (GRR).

References

1. Blom, J. G. and Verwer, J. G., 1993, VLUGR2: a Vectorised Local Uniform Grid Refinement Code for PDEs in 2D, Report NM-R9306, CWI, Amsterdam.
2. Childs, T. H. C. and Juster, N. P., 1994, Linear and Geometric Accuracies from Layer Manufacturing, Annals CIRP, 43/1: 163-166.
3. Childs, T. H. C., Cardie, S. and Brown, J. M., 1994, Selective Laer Sintering of Polycarbonate at Varying Powers, Scan Speeds and Scan Spacings, Proc. 5th SFFF Symposium, 356-363, University of Austin, Texas.
4. Jaeger, J. C., 1942, Jnl. Roy. Soc. New South Wales, 76: 203-2224.
5. Kruth, J. P., 1991, Material Incress Manufacturing by Rapid Prototyping Techniques, Annals CIRP, 40/2: 603-614.
6. Nelson, J. C. et al., 1993, Model of the Selective Laser Sintering of Bisphenol-A Polycarbonate, Ind. Eng. Chem. Res., 32: 2305-2317.